CP-odd phase correlations and electric dipole moments

Keith A. Olive,[1] Maxim Pospelov,[2,3,4] Adam Ritz,[5] and Yudi Santoso[2,3]

[1]*W. I. Fine Theoretical Physics Institute, School of Physics
and Astronomy, University of Minnesota, Minneapolis, Minnesota 55455, USA*
[2]*Department of Physics, University of Guelph, Guelph, Ontario N1G 2W1, Canada*
[3]*Perimeter Institute for Theoretical Physics, Waterloo, Ontario N2J 2W9, Canada*
[4]*Department of Physics and Astronomy, University of Victoria, Victoria, BC, V8P 1A1 Canada*
[5]*Theoretical Division, Department of Physics, CERN, Geneva 23, CH-1211 Switzerland*

We revisit the constraints imposed by electric dipole moments (EDMs) of nucleons and heavy atoms on new *CP*-violating sources within supersymmetric theories. We point out that certain two-loop renormalization group corrections induce significant mixing between the basis-invariant *CP*-odd phases. In the framework of the constrained minimal supersymmetric standard model, the *CP*-odd invariant related to the soft trilinear *A*-phase at the grand unified theory (GUT) scale, θ_A, induces nontrivial and distinct *CP*-odd phases for the three gaugino masses at the weak scale. The latter give one-loop contributions to EDMs enhanced by $\tan\beta$, and can provide the dominant contribution to the electron EDM induced by θ_A. We perform a detailed analysis of the EDM constraints within the constrained minimal supersymmetric standard model, exhibiting the reach, in terms of sparticle spectra, which may be obtained assuming generic phases, as well as the limits on the *CP*-odd phases for some specific parameter points where detailed phenomenological studies are available. We also illustrate how this reach will expand with results from the next generation of experiments which are currently in development.

I. INTRODUCTION

Electric dipole moments (EDMs) of the neutron [1] and heavy atoms and molecules [2–8] are primary observables in probing for sources of flavor-neutral *CP* violation. The high degree of precision with which various experiments have put limits on possible EDMs translates into stringent constraints on a variety of extensions of the standard model at and above the electroweak scale (see, e.g. [9]). Currently, the strongest constraints on *CP*-violating parameters arise from the atomic EDMs of thallium [2] and mercury [3], and that of the neutron [1]:

$$|d_{\text{Tl}}| < 9 \times 10^{-25} e \, \text{cm} \qquad |d_{\text{Hg}}| < 2 \times 10^{-28} e \, \text{cm}$$
$$|d_n| < 6 \times 10^{-26} e \, \text{cm}. \qquad (1.1)$$

When interpreted as a quantity induced purely by the electron EDM d_e, the measurement of d_{Tl} can be translated into a tight bound, $|d_e| < 1.6 \times 10^{-27} e \, \text{cm}$.

While the standard model paradigm of the Cabibbo-Kobayashi-Maskawa quark-mixing matrix (CKM) has received remarkable overall confirmation with the observation of *CP*-violation in the mixing and decays of neutral *B*-mesons, the motivation for anticipating new sources of *CP*-violation is undiminished. This is in part through the need to explain baryogenesis, and also through the generic appearance of new *CP*-violating phases in models of new physics introduced to stabilize the Higgs sector. In particular, supersymmetric models with minimal field content, i.e. the minimal supersymmetric standard model (MSSM), allow for the presence of several *CP*-violating phases even in the most restrictive ansatz of flavor universality

in the squark and slepton sectors. The null experimental EDM results pose a serious problem for the MSSM with superpartner masses around the (natural) electroweak scale. Indeed, a typical *CP*-violating supersymmetry (SUSY) phase of order one combined with $\mathcal{O}(100 \, \text{GeV})$ masses for the superpartners would violate experimental constraints by up to 3 orders of magnitude [10]. Moreover, ongoing and planned EDM experiments are aiming to improve the level of sensitivity to underlying *CP*-odd sources by several additional orders of magnitude.

Over the years the SUSY *CP* problem has led to a number of suggestions for how this tuning might be alleviated:

small phases: The simplest solution in principle is of course just to demand that the diagonal phases are small (or zero). However, a framework with small phases would run counter to the natural standard model interpretation of *CP*-violation in the mixing and decays of *B*-mesons, which requires no analogous tuning. Of course, such a scenario is possible, e.g. in the framework of spontaneous *CP*-violation [11,12], but requires a significant amount of model building, particularly in terms of constraints on the flavor structure, in order to suppress the flavor-diagonal phases while allowing the effective CKM phase to be order one.

flavor off-diagonal *CP*-violation: As a principle to motivate small diagonal phases, one may interpret the EDM constraints, in concert with the success of the CKM paradigm, as implying that certain symmetries should ensure that all *CP*-violation arises via an interplay with flavor structures. This is an appealing viewpoint, and can be taken as motivation to try and divorce

CP-violation from the SUSY-breaking sector. However, even in the case that the soft terms are real, any significant nonuniversality in these terms, i.e. misalignment between the *A* terms and the Yukawas, will generically lead to large EDMs via the large *CP*-violating phases in the Yukawa matrices (see e.g. [13]). Thus, even within this seemingly rather restrictive scenario, further constraints must be imposed either on the flavor sector [14] or the SUSY-breaking sector to lessen the impact from the EDM constraints.

cancellations: The MSSM contains in principle many new *CP*-violating phases, and while a lot of these are highly constrained by the flavor sector, there are still several new flavor-diagonal phases. Indeed, there are more phases than experimental EDM observables with which to bound them, and thus various partial cancellations and degeneracies are to be expected [15–18]. However, the most recent analyses [19–21] using a generic set of flavor-diagonal phases and the three competitive EDM bounds suggest that such cancellations are difficult to achieve if at all.

decoupling: One can clearly reduce the constraints by lifting the scale of the superpartners [22]. If one only considers the leading one-loop contributions to the EDMs, this can be done in ways that do not significantly affect the level of tuning in the Higgs sector, i.e. by keeping the 3rd generation scalars light, as is also required by cosmological constraints [23]. However, various subleading effects then come into play and limit the extent to which the EDMs can be suppressed. One of our goals here will be to map out precisely how far EDMs can reach in terms of the superpartner scale.

Taken as a whole, one may observe that these scenarios could allow for various partial suppressions of the EDMs but, although various models exists, within the generic supersymmetric framework we currently lack a compelling symmetry argument for why the EDMs should be suppressed by many orders of magnitude as they are in the standard model. Thus, with the current level of experimental progress, we can expect many of these scenarios to be put to the test in the coming few years, providing ample motivation for further theoretical consideration of the EDM sensitivities.

To summarize the current situation, recall that on restricting attention to the framework of the constrained MSSM [24,25], one reduces the number of new fundamental phases to two, which can be chosen to be the phases of the *A* and μ parameters at the GUT scale. It is well known that the phase of μ is particularly effective in inducing EDMs, and, therefore, for reasonably generic sparticle spectra is tightly constrained, while the phase of *A* can in principle be maximal (See e.g. [15]). For example, this may be explained by the tanβ-enhancement of the one-loop EDMs induced by the phase of μ, while the corresponding enhancement of the *A*-phase arises only at the two-loop level. In fact, as we shall discuss below, this

argument is far from watertight as other contributions can also be important.

The present work has three main goals. The first, and more technical, goal is to update the calculation of the EDMs by including certain two-loop corrections in the running of the soft-breaking parameters from the GUT to the weak scale. At first sight, the inclusion of the two-loop running should not substantially change the prediction for EDMs in terms of the SUSY phases. However, a complex *A* parameter induces imaginary corrections to the gaugino masses, which then induce the EDMs via one-loop SUSY threshold diagrams that are enhanced by tanβ. This significantly modifies the EDM predictions as a function of the *A*-phase at the GUT scale and remarkably enough, in the case of even moderate tanβ, these new contributions can provide the dominate source for the electron EDM.

The second goal of the paper is to present an updated and complete analysis of the constraints imposed by EDMs on the parameter space of the constrained MSSM (CMSSM). We focus on the CMSSM in order to incorporate full phenomenological analyses. However, for various reasons it seems that relaxing the universality assumption does not in fact significantly alter the conclusions [20,21], although this issue perhaps deserves further attention. We will update the corresponding results of [20,21], by incorporating the new Tl-EDM bound and most significantly by treating the qualitatively distinct large tanβ regime, utilizing the results of [26]. The third and final goal is to emphasize the significant improvements in sensitivity, by orders of magnitude in most cases, that are likely within a few years due to the current and next-generation EDM searches.

The paper is organized as follows. In the next section we detail the new contributions to the EDMs induced primarily by two-loop running of the soft-breaking parameters. In Sec. III, for completeness we give a short summary of the EDM formulas that relate the observables to the Wilson coefficients of the *CP*-odd effective Lagrangian, which are in turn determined by SUSY diagrams. We also outline the anticipated sensitivity of the next-generation EDM experiments. Section IV describes the numerical analysis within the CMSSM framework, and presents the limits on *CP*-violating phases as well as the potential reach of EDMs in terms of the SUSY mass spectrum. Some concluding remarks appear in Sec. V.

II. RG EVOLUTION OF THE *CP*-ODD INVARIANTS AT TWO LOOPS

We begin by exhibiting a simplified formula for the one-loop contributions to the electron EDM in terms of the *CP*-violating SUSY phases [19],

$$d_e = \frac{em_e}{16\pi^2 M_{\mathrm{SUSY}}^2}\Bigg[\left(\frac{5g_2^2}{24} + \frac{g_1^2}{24}\right)\tan\beta\,\sin[\mathrm{Arg}(\mu M_2 m_{12}^{2*})]$$
$$+ \frac{g_1^2}{12}\sin[\mathrm{Arg}(M_1^* A_e)]\Bigg], \tag{2.1}$$

where $M_1(M_2)$ are the U(1)(SU(2)) gaugino masses, all the couplings and masses are normalized at the weak scale, and we chose a SUSY parameter point with the absolute value of all soft-breaking parameters in the selectron and gaugino sector equal to M_{SUSY}. This leads to a transparent overall normalization for d_e. The soft-breaking parameter in the Higgs sector, m_{12}^2, enters Eq. (2.1) via the relative phase of the two Higgs vacuum expectation values. It is possible to choose m_{12}^2 (also denoted $B\mu$ or b in an alternative notation) and consequently v_1 and v_2 to be real. It is easy to see why the phases of μ and the Wino mass give larger contributions to d_e than does the phase of A. For example,

$$\frac{d_e(\theta_\mu, \theta_{M_2})}{d_e(\theta_{A_e}, \theta_{M_1})} \simeq \frac{5g_2^2}{2g_1^2} \tan\beta \frac{\sin(\theta_\mu + \theta_{M_2})}{\sin(\theta_{A_e} - \theta_{M_1})}$$

$$\simeq 10 \tan\beta \frac{\sin(\theta_\mu + \theta_{M_2})}{\sin(\theta_{A_e} - \theta_{M_1})}, \qquad (2.2)$$

which implies that the sensitivity to the phase of μ is enhanced by 2 orders of magnitude relative to the phase of A, even for moderate values of $\tan\beta$. For hadronic EDMs this effect is also present, although the advantage of θ_μ is less pronounced because both phases can generate EDMs proportional to g_3^2. The enhancement (2.2) provides the primary explanation for why the phase of μ is more severely constrained than the phases of the A-parameters.

Even with the restrictions of flavor universality and proportionality, the number of independent *CP*-odd phases can be rather large. Working within the CMSSM scenario, one assumes a common phase for the trilinear parameters at the GUT scale, and a common phase for the gaugino masses. This reduces the number of physical *CP*-odd phases to two and a traditional choice of basis at the GUT scale comprises θ_μ and θ_A:

$$(\theta_A \equiv \mathrm{Arg}(A_f), \qquad \theta_\mu \equiv \mathrm{Arg}(\mu)); \qquad (2.3)$$

$$\mathrm{Arg}(M_i) = 0;$$
$$\theta_{12} \equiv \mathrm{Arg}(m_{12}^2) \text{ -tuned to ensure } \mathrm{Arg}(m_{12}^2)_{EW} = 0. \qquad (2.4)$$

The utility of this basis lies in the invariance of the $\mathrm{Arg}(M_i) = 0$ condition under one-loop renormalization group evolution, and also the invariance of θ_μ. If needed, the basis (2.4) can be rotated to any other convenient basis in the CMSSM framework by appropriate phase redefinitions of the matter and gauge superfields. The choice of $\mathrm{Arg}(m_{12}^2)$ at the GUT scale, which is *not* invariant under RG evolution [16,27], is such as to ensure the reality of the Higgs vacuum expectation values (vevs). Thus, choosing different values for θ_μ and θ_A requires a readjustment of θ_{12} at the GUT scale in these conventions which, although aesthetically unappealing, simplifies calculations by eliminating the dependence on θ_{12} of the EDMs.

A. Further contributions to $d_e(\theta_A)$

With this basis in mind, consider the relative enhancement of the $(\theta_\mu + \theta_{M_2})$ contribution to d_e as apparent in (2.2). One observes that for moderate values of $\tan\beta$ it is sufficiently large to counteract a further loop suppression factor. Thus, in the absence of a μ-phase, one may enquire whether higher-loop corrections, induced by θ_A, may become sizable in this way at large $\tan\beta$ and compete with the standard one-loop contribution to $d_e(\theta_A)$. A number of 2-loop threshold corrections to the fermion EDMs have been considered in the MSSM literature, notably supersymmetric variants of the Barr-Zee diagrams [28] which involve the Higgs sector. However, a number of other corrections of this type exist. Indeed, its clear that top-stop threshold corrections on the gaugino line, as shown for d_d in Fig. 1(a), may give a $\tan\beta$-enhanced contribution to fermion EDMs $d_f(\theta_{A_t})$ and quark color EDMs (CEDMs) $\tilde{d}_q(\theta_{A_t})$. However, its relative size compared to the conventional one-loop term, ignoring hierarchies in μ and A, is of order $\tan\beta(m_t/m_{\tilde{t}})^2/(16\pi^2)$, and thus not particularly sizable.

These corrections would clearly be much more important in the case of d_e were it possible for a dependence on θ_A to manifest itself via the chargino diagram, and make full use of the enhancement factor of $\mathcal{O}(10\tan\beta)$ in (2.2). Threshold corrections of this type were noted by Pilaftsis [29], and the most prominent example is shown in Fig. 1(b). The internal stop-bottom loop provides a complex wave function correction of order $\Sigma \sim m_t A_t^*/(16\pi^2 m_{\tilde{t}}^2)$ which mixes $\tilde{H}_2$ with $\tilde{W}^+$. Taking the limit where the stops are heavy, the resulting contribution to d_e scales as $\Delta d_e \sim m_e \tan\beta \mathrm{Im}(A_t)/((16\pi^2 m_{\tilde{t}})^2 \mu)$, which, despite the loop suppression, can be comparable with, or even larger than, the 1-loop neutralino diagram. Moreover, such contributions are often considerably larger than the more widely known Barr-Zee type diagrams, and deserve to be included in more general analyses. However, in the restricted framework of the CMSSM, while competitive with other contributions, they are somewhat suppressed by RG effects which generically render the ratio $\mathrm{Im}(A_t)m_t/m_{\tilde{t}}^2$ rather small at the weak scale. Indeed, we will not need to study them in detail because, remarkably enough, it turns out that there is an even larger class of contributions which are less sensitive to detailed features of the spectrum.

In particular, one can consider a diagram where in the top-stop loop, e.g. of Fig. 1(a), we tie the Higgs lines together to generate a two-loop correction to the running of the gluino mass. While further loop suppressed, this diagram is enhanced by a large RG log and the relative contribution of such a diagram compared to Fig. 1(a) is of order $\ln(\mu_{GUT}/M_Z)(m_{\tilde{t}}/m_t)^2/(16\pi^2)$, which can easily be greater than one. In the case of quark EDMs, such corrections are still generally negligible. However, when such RG corrections are accounted for on the Wino line of the
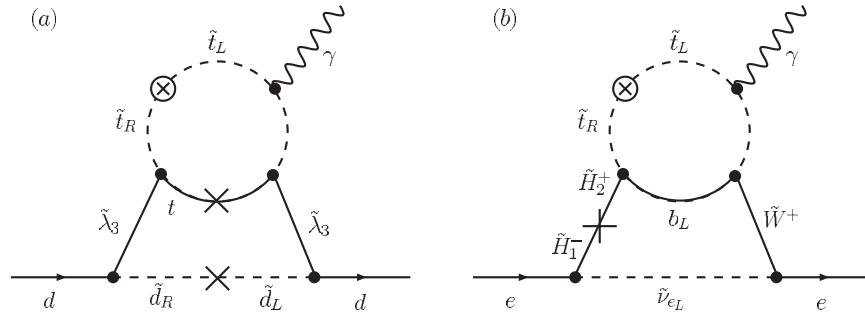
FIG. 1. On the left is an example of a $\tan\beta$-enhanced two-loop threshold correction to $d_d(\theta_A)$. If μ is real, the phase enters via the circled left-right stop insertion. On the right we show a more significant $\tan\beta$-enhanced threshold correction to $d_e(\theta_A)$ [29].
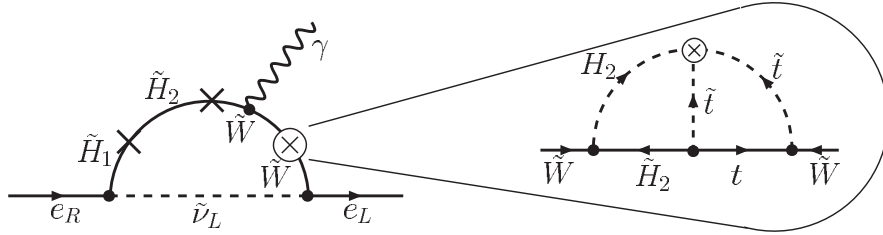

FIG. 2. A two-loop RG correction to $\mathrm{Im}M_2$, induced by θ_A which contributes to $d_e(\theta_A)$ via the chargino threshold diagram (shown in the mass-insertion approximation). Despite the loop suppression, the result is enhanced by $\tan\beta$, a large RG log, and a ratio of couplings, and thus can be larger than the one-loop neutralino contribution as discussed in the text.

chargino diagram, the corrections to $d_e(\theta_A)$ as shown in Fig. 2 can be sizable. Despite the large loop suppression, it benefits from the enhancement factor in (2.2), a large RG log, and since the insertion is divergent it is not suppressed by the generically large squark masses. Remarkably, within the CMSSM and for moderate-to-large $\tan\beta$, it seems that this 3-loop effect can easily be larger than the leading 1-loop threshold correction to $d_e(\theta_A)$, and also the 2-loop threshold corrections in Fig. 1(b). Thus it will have important consequences for the EDMs, as we will now discuss more quantitatively below.

B. Two-loop RG evolution and EDMs

To be more precise, at two-loop order, imaginary corrections to the gaugino masses may be generated if $\mathrm{Im}A$ is nonzero. The corresponding part of the RG equation for M_i [30],

$$\frac{d}{dt}\mathrm{Im}(M_i) = \frac{2g_i^2}{(16\pi^2)^2}\sum_{f=u,d,e} C_i^f \mathrm{Im}(A_f)\mathrm{Tr}(\mathbf{Y}_f^\dagger \mathbf{Y}_f), \quad (2.5)$$

with (in the $\overline{\mathrm{DR}}$ scheme)

$$C_i^f = \begin{pmatrix} 26/5 & 14/5 & 18/5 \\ 6 & 6 & 2 \\ 4 & 4 & 0 \end{pmatrix}, \quad (2.6)$$

spans all the flavors, but is dominated by the top, and for large $\tan\beta$ bottom and tau, contributions.

While we will not attempt a full treatment of the two-loop RG equations, we will take into account the relevant contributions that generate $\mathrm{Im}(M_i)$ at the weak scale. In order to estimate the order of magnitude of this effect, we can consider a simple scenario where we focus on the evolution of M_2, and retain only the largest (top) Yukawa term. One then finds, $(d/dt)\mathrm{Im}(M_2) \simeq 3Y_t^2\alpha_2/(16\pi^3)\mathrm{Im}(A)$, which to leading-log order integrates to

$$\mathrm{Im}(M_2(M_Z)) \simeq -\frac{3\alpha_2(\mu_{\mathrm{GUT}})}{32\pi^3}\mathrm{Im}(A_0)\ln\left(\frac{\mu_{\mathrm{GUT}}^2}{M_Z^2}\right)$$

$$\sim -6\times 10^{-3}\mathrm{Im}(A_0), \quad (2.7)$$

where we have inserted the GUT-scale value for α_2, but used the weak-scale value for Y_t. This estimate, which accounts only for the top-stop contribution, provides a reasonably accurate approximation for most regimes. The two-loop suppression factor indicates why resummation of the large logs does not change the result significantly. Written in basis-independent form, the estimate (2.7) expresses corrections to three weak scale CP-odd invariants, $\mathrm{Arg}(\mu M_i m_{12}^{2*})$, as a function of the GUT-scale invariants $\mathrm{Arg}(M_i A)$.

As noted above, a particular example of the relevant contributions to the EDMs is shown explicitly in Fig. 2. It combines the two-loop running of the soft parameters with the one-loop SUSY threshold contribution to the EDM. It is clear that to a certain degree the effect of $\mathrm{Im}(M_i)$ mimics

$\text{Im}(\mu)$ inside such a diagram, and thus is most prominent when $\vec{\theta}_{\text{GUT}} \equiv (\theta_\mu, \theta_A) = (0, \theta_A)$. These contributions are clearly also present for quark EDMs and CEDMs, but as discussed above are less competitive as the corresponding enhancement factor is an order of magnitude smaller than (2.2).

The result (2.7) has a significant effect on the calculation of EDMs induced by θ_A for several reasons:

(i) The two-loop running destroys the universality of the gaugino mass phases at the weak scale, which therefore have to be taken into account in EDM calculations.

(ii) The resulting size of the imaginary parts of M_i appears to be small, $O(10^{-2}\text{–}10^{-3}) \times M_{\text{SUSY}}$ (2.7). However, in combination with the enhancement factor $\sim 10 \tan\beta$ (2.2), the resulting correction to d_e can be $O(1\text{–}10)$, for moderate-to-large $\tan\beta$, as compared to the "standard" result for $d_e(\theta_A)$.

(iii) The two-loop RG-induced correction to $d_e(\theta_A)$ has the opposite sign relative to the standard result, providing a regime where the two contributions can cancel each other.

Putting together the various numerical factors, from RG-running and the SUSY threshold-induced EDM, we see that the new contributions induced by $\text{Im}(M_i(\theta_A))$ correspond to a three-loop correction which is enhanced by $\mathcal{O}(1\text{–}10) \tan\beta \times \ln(\mu_{\text{GUT}}^2/M_Z^2)$, and as emphasized above is often larger than the leading 1-loop threshold correction and various additional 2-loop threshold corrections. The question then arises as to whether there are other three-loop effects with a comparable enhancement, i.e. $\propto \tan^2\beta$. It is well known, however, that such contributions do not exist. Enhancement by a single power of $\tan\beta$ results from $d_e \propto y_e \langle H_2 \rangle \propto m_e \tan\beta$. Any additional power of $\tan\beta$ can arise only from additional insertions of the Yukawa couplings of charged leptons or down-type quarks, which cannot lead to a numerical enhancement.

III. AN EDM SUMMARY

In this section, we briefly recall the dependence of the observable EDMs on the most significant flavor-diagonal *CP*-odd operators at 1 GeV (see [31] for a recent review). Up to dimension six, the corresponding effective Lagrangian takes the form

$$
\begin{aligned}
\mathcal{L}_{\text{eff}} = {} & \frac{g_s^2}{32\pi^2} \bar{\theta} G_{\mu\nu}^a \tilde{G}^{\mu\nu,a} - \frac{i}{2} \sum_{i=e,u,d,s} d_i \bar{\psi}_i (F\sigma) \gamma_5 \psi_i \\
& - \frac{i}{2} \sum_{i=u,d,s} \tilde{d}_i \bar{\psi}_i g_s (G\sigma) \gamma_5 \psi_i \\
& + \frac{1}{3} w f^{abc} G_{\mu\nu}^a \tilde{G}^{\nu\beta,b} G_\beta^{\mu,c} \\
& + \sum_{i,j} C_{ij} (\bar{\psi}_i \psi_i)(\psi_j i \gamma_5 \psi_j) + \cdots
\end{aligned}
\tag{3.1}
$$

For the four-fermion operators, the sum runs over all light fermions, and one could in principle include additional tensor structures [32–35]. In practice, since these operators require a double helicity flip, implying additional $(m_q/v_{\text{EW}})^2$ suppression factors, they are generally negligible. The exception to this rule is at large $\tan\beta$, where C_{ij} grow as $(\tan\beta)^3$, and they can compete with the other sources in certain parameter regimes [26,36].

In supersymmetric models with *CP*-violating phases larger than $\sim 10^{-8}$ in the flavor-diagonal sector, the only reasonable strategy to avoid the strong *CP* problem is to postulate the existence of the Peccei-Quinn (PQ) relaxation mechanism [37], which removes the theta term from the list of contributing operators. We will adopt this strategy here.

We will now turn to a quick synopsis of the dependence of the observable EDMs on the remaining dimension five and six operators. The physical observables can be conveniently separated into three main categories, depending on the physical mechanisms via which an EDM can be generated: EDMs of paramagnetic atoms and molecules, EDMs of diamagnetic atoms, and the neutron EDM.

A. EDMs of paramagnetic atoms—thallium EDM

Among various paramagnetic systems, the EDM of the thallium atom currently provides the best constraints. Atomic calculations [38–40] (see also Ref. [9] for a more complete list) link the atomic EDM with d_e and various *CP*-odd electron-nucleon interactions, of which we shall only consider the most relevant, namely $C_S \bar{e} i \gamma_5 e \bar{N} N$,

$$
d_{\text{Tl}} = -585 d_e - e 43 \text{ GeV} C_S^{\text{sing}},
\tag{3.2}
$$

where we have furthermore retained only the leading iso-singlet component of C_S. The relevant atomic matrix elements are calculated to within 10%–20% accuracy [41].[1]

The dependence of C_S on the four-fermion sources C_{ie}, for $i = d, s, b$, can be expressed in the form [26,36],

$$
\begin{aligned}
C_S^{\text{sing}} = {} & C_{de} \frac{29 \text{ MeV}}{m_d} + C_{se} \frac{\kappa \times 220 \text{ MeV}}{m_s} \\
& + C_{be} \frac{66 \text{ MeV}(1 - 0.25\kappa)}{m_b},
\end{aligned}
\tag{3.3}
$$

where $\kappa \equiv \langle N | m_s \bar{s} s | N \rangle / 220 \text{ MeV}$, and we will adopt the value obtained using NLO χPT, $\kappa \sim 0.50 \pm 0.25$ [42]. Larger values for the pion-nucleon sigma term $\sigma_{\pi N}$, advo-

---

[1] It is worth emphasizing that, due to the contributions from C_S, a bound on more than one paramagnetic species is required to infer a direct bound on d_e. Thus, a conservative and model-independent bound on d_e cannot be derived from the bound on d_{Tl} alone, and would be ~ 2 orders of magnitude weaker than the commonly quoted value obtained by dropping the dependence on C_S in (3.2).

cated recently (see e.g. [43]), would result in a somewhat larger value for $\kappa \sim 1.55$.

B. Neutron EDM

The calculation of the neutron EDM in terms of the Wilson coefficients of Eq. (3.1) represents a difficult non-perturbative problem, and thus the precision currently obtainable is not competitive with the results outlined above for $d_{\rm Tl}$. Nonetheless, d_n plays a crucial role in constraining CP-odd sources in the quark sector, and we will make use of the results obtained using QCD sum rule techniques [44,45] (see [19,46–48] for alternative approaches using chiral techniques), that we briefly recall below.

In the presence of the PQ mechanism, it is natural to expect that the dominant contribution to the neutron EDM comes from the EDMs and CEDMs of the light quarks. Within the sum-rules framework, PQ relaxation also suppresses the sea-quark contribution at leading order, and leads to the following result [44]:

$$d_n(d_q, \tilde{d}_q) = (1.4 \pm 0.6)(d_d - 0.25 d_u)$$
$$+ (1.1 \pm 0.5)e(\tilde{d}_d + 0.5\tilde{d}_u). \quad (3.4)$$

The quark vacuum condensate, $\langle \bar{q}q \rangle = (225 \text{ MeV})^3$, has been used in this relation—the proportionality to $d_q \langle \bar{q}q \rangle \sim m_q \langle \bar{q}q \rangle \sim f_\pi^2 m_\pi^2$ removes any sensitivity to the poorly known absolute value of the light quark masses. Here $\tilde{d}_q$ and d_q are to be normalized at the hadronic scale which we assume to be 1 GeV. Note also that the quark masses used for the SUSY calculations of d_q and $\tilde{d}_q$ should be taken at the weak scale, where their numerical values are smaller than the low energy values by a factor of ~ 0.35, e.g. $m_d(M_Z) \simeq 9.5 \text{ MeV} \times 0.35$.

The dimension six sources, w and $C_{q_1 q_2}$, also contribute to the neutron EDM but are more problematic to handle within the sum-rules framework. One can nonetheless obtain estimates that are useful for assessing the regimes in which the contributions in (3.4) are dominant. One finds [45]

$$d_n(w) \sim 20 \text{ MeV} \times ew. \quad (3.5)$$

This estimate is assessed to be valid within a factor of 2–3 [45]. When $\tan\beta$ is large, the dominant contributions to w arise via threshold corrections from the CEDMs of heavy quarks [49,50], e.g. $\delta w(\tilde{d}_b) \simeq g_s^3 \tilde{d}_b(m_b)/(32\pi^2 m_b)$.

In general there are also many possible contributions from four-fermion sources. However, since these contribute only at large $\tan\beta$, the most relevant are $C_{bd} \simeq -C_{db}$ and $C_{sb} \simeq -C_{bs}$. In this case, one can obtain an estimate of the form [26]

$$d_n(C_{bd}) \sim e 0.7 \times 10^{-3} \text{ GeV}^2 \frac{C_{bd}}{m_b}, \quad (3.6)$$

which again is primarily useful as a means to estimate regimes where large corrections to (3.4) are possible.

C. EDMs of diamagnetic atoms—mercury EDM

EDMs of diamagnetic atoms, i.e. atoms with total electron angular momentum equal to zero, also provide an important test of CP violation [9]. The current limit on the EDM of mercury [3] furnishes one of the most sensitive constraints on SUSY CP-violating phases [19]. However, the calculation of $d_{\rm Hg}$ is undoubtedly the most difficult as it requires QCD, nuclear, and also atomic input.

The atomic EDM of mercury arises from several important sources, namely, the Schiff moment S [51], the electron EDM d_e, and also electron-nucleon interactions (see, e.g. Ref. [9] for a comprehensive review). Schematically, the mercury EDM can be represented as

$$d_{\rm Hg} = d_{\rm Hg}(S[\bar{g}_{\pi NN}(\tilde{d}_i, C_{q_1 q_2})], C_S[C_{qe}], C_P[C_{eq}], d_e), \quad (3.7)$$

where $\bar{g}_{\pi NN}$ collectively denotes the CP-odd pion-nucleon couplings, and C_S and C_P denote, respectively, the couplings $\bar{e}i\gamma_5 e\bar{N}N$ and $\bar{e}e\bar{N}i\gamma_5 N$. The Weinberg operator does not provide any appreciable contribution to $d_{\rm Hg}$ because its contribution to $\bar{g}_{\pi NN}$ is suppressed by an additional chiral factor of $m_q/1 \text{ GeV} \sim 10^{-2}$.

A number of the atomic and nuclear components of the calculation have been updated recently, specifically $d_{\rm Hg}(S)$ [52] and $S(\bar{g}_{\pi NN})$ [53]. We will also make use of an updated result for $\bar{g}_{\pi NN}(\tilde{d}_i)$ obtained by combining chiral and sum-rules techniques [54],

$$\bar{g}_{\pi NN}^{(1)}(\tilde{d}_q) \sim 4^{+8}_{-2}(\tilde{d}_u - \tilde{d}_d)[\text{GeV}^{-1}], \quad (3.8)$$

where the relatively large overall uncertainty arises from significant cancellations between the leading contributions. Combining this result with the contribution of four-fermion operators [26], and the atomic and nuclear parts of the calculation, we obtain

$$d_{\rm Hg} = 7 \times 10^{-3} e(\tilde{d}_u - \tilde{d}_d) + 10^{-2} d_e$$
$$- 1.4 \times 10^{-5} e \text{ GeV}^2 \left(\frac{0.5 C_{dd}}{m_d} + 3.3\kappa \frac{C_{sd}}{m_s} \right.$$
$$\left. + \frac{C_{bd}}{m_b}(1 - 0.25\kappa) \right) + 3.5 \times 10^{-3} \text{ GeV} eC_S$$
$$+ 4 \times 10^{-4} \text{ GeV} eC_P. \quad (3.9)$$

The contributions in the second and third lines are significant in the MSSM only for large $\tan\beta$.

The most valuable feature of $d_{\rm Hg}$ is its sensitivity to the triplet combination of CEDM operators $\tilde{d}_i$, which surpasses the sensitivity of the neutron EDM to this combination by a factor of a few. Moreover, despite the fact that the overall coefficient is only known with relatively poor precision, the dominant dependence on the $(\tilde{d}_u - \tilde{d}_d)$ com-

bination ensures that these uncertainties enter as an overall factor and therefore do not significantly alter the shape of the unconstrained band of the parameter space in the $\theta_\mu - \theta_A$ plane.

D. Future experimental sensitivity

The experimental situation is currently very active, and a number of new EDM experiments are already in development which promise to significantly improve the level of sensitivity by several orders of magnitude in the next few years. As part of our analysis in the next section, we will present the reach of these next-generation experiments within the CMSSM, given the following assumed sensitivity in the three classes of EDMs on which we have been focusing:

$$|\Delta d_e| < 3 \times 10^{-29} e \text{ cm} \qquad |\Delta d_D| < 2 \times 10^{-27} e \text{ cm}$$
$$|\Delta d_n| < 1 \times 10^{-27} e \text{ cm}. \qquad (3.10)$$

These sensitivities were chosen conservatively according to expectations for the first physics runs of the relevant experiments discussed below. It is possible that the ultimate sensitivity will be at least an order of magnitude better in most cases.

The first constraint shown in (3.10) corresponds to a relatively conservative estimate of the sensitivity achievable within three active projects utilizing, respectively, two polarizable paramagnetic molecules, PbO [8] and YbF [7], and also a solid state system [55]. The first two of these primarily obtain their enhanced sensitivity from the fact that the internal electric field, to which the electron EDM is sensitive, is further enhanced by the polarization of the molecule. One should bear in mind that, as for Tl, these experiments do not directly bound d_e and electron-nucleon operators may also be relevant. PbO and YbF are polarized by the external field in a nonlinear way and thus do not have EDMs as such. However, the induced shift in the Larmor precession frequency can still be written in the form

$$\hbar \Delta \omega_L \sim \mathcal{E}_{\text{eff}} d_e + \mathcal{O}(C_S). \qquad (3.11)$$

We are not aware of any calculations for the C_S-dependence in this case, while the quoted sensitivity in (3.10) comes from ignoring this term and using estimates for the effective field $\mathcal{E}_{\text{eff}}$ [56] and the sensitivity to ω_L [7,8]. As alluded to above, if no further systematic issues arise, the final sensitivity could in fact be several orders of magnitude better than this quoted result [8,55]. Given that the relevant atomic calculations are only partially completed, we will simply scale up the result for Tl and restrict ourselves to a relatively low value of $\tan\beta$, in order to ameliorate the problem of unknown corrections from C_S. Nonetheless, one should be aware that the molecular matrix element relating C_S and ω_L, although enhanced by the same factor Z^3, will not be a simple rescaling

of the Tl result, and thus the final dependency $\omega_L(d_e, C_S)$ may be somewhat different from $d_{\text{Tl}}(d_e, C_S)$. Clearly further progress on atomic calculations for this system would be welcome.

The second constraint in (3.10), refers to the proposed search for the deuteron EDM using the BNL storage ring [57]. This proposal seems our best chance for significant improvement in the diamagnetic sector. The deuteron is not a diamagnetic system of course, but the EDM turns out to be primarily sensitive to $\bar{g}_{\pi NN}^{(1)}$ (assuming $\bar{\theta}$ is removed by PQ rotation) [58–60],

$$d_D \simeq d_n + d_p - (1.3 \pm 0.3) e \bar{g}_{\pi NN}^{(1)} (\tilde{d}_q) [\text{GeV}^{-1}] \quad (3.12)$$

and thus it plays a similar role in terms of its sensitivity to underlying CP-odd sources. Indeed, it has the significant advantage in this regard of not requiring complicated many-body nuclear calculations.

The final constraint in (3.10) refers to the expected (initial) sensitivity of several experiments currently in development, at LANSCE [61], at ILL [62], and at PSI [63], searching for an EDM of the neutron. The ultimate sensitivity could again be an order of magnitude better.

IV. NUMERICAL RESULTS AND EDM CONSTRAINTS

Before we turn to the numerical analysis of EDMs within the CMSSM framework, for completeness we now list the relevant SUSY contributions to the operators in (3.1) that must be included:

A. SUSY contributions to CP-odd higher-dimensional operators

Within the effective theory formulated at the weak scale, or rather the mass scale of the superpartners, the CP-odd operators in (3.1) can be induced by the following threshold corrections, all of which we will include in our analysis.

1. Fermion EDMs and CEDMs

1-loop.—At one-loop order the electron EDM receives contributions from $\tilde{\chi}^- - \tilde{\nu}_e$ and $\tilde{\chi}^0 - \tilde{e}^-$ loops (see e.g. [17]). The EDMs and CEDMs of quarks receive analogous contributions, and in addition have generically dominant contributions from gluino-squark loops (see e.g. [17]). As we argued in Sec. II, these one-loop results *must* be formulated in the basis where ImM_i at the weak scale are taken into account.

2-loop.—At 2-loop order, non-negligible Barr-Zee-type Higgs-mediated graphs contribute to EDMs and CEDMs [28]. The induced photon couplings, e.g. AFF and $HF\tilde{F}$, arise through sfermion and chargino loops, with dominant contributions from stop (and, for large $\tan\beta$, sbottom, and

stau [26]) loops. These diagrams can be significant when the first generation sfermions are heavy.[2]

2. Weinberg operator

2-loop.—The Weinberg operator [64] also contributes to d_n via two-loop stop-top-gluino contributions (see e.g. [17]), particularly in the regime where the first generation sfermions are heavy. As noted earlier, the Weinberg operator may also receive non-negligible corrections from heavy quark CEDMs under RG evolution to low scales [26,49,50].

3. Four-fermion operators

1-loop.—We account for the leading $\tan\beta$-enhanced contributions [36], as computed in [26], induced by scalar or pseudoscalar Higgs exchange, with a $\tan\beta$-enhanced coupling of down-type fermions to H_2 induced by various 1-loop threshold corrections. There are also similar Higgs exchange contributions with loop-induced $H - A$ mixing that are generically subdominant.

These contributions are quite generic in any SUSY model of new physics at the TeV scale. We turn now to a numerical analysis of the EDM sensitivity to phases and SUSY masses within the framework of the CMSSM.

B. EDM reach and constraints on *CP*-odd phases in CMSSM

In this section we analyze all three observables, d_{Tl}, d_n, and d_{Hg}, within the CMSSM, defined by the following set of universal SUSY parameters at the GUT scale:

$$\{\tan\beta, m_0, m_{1/2}, |A_0|, \theta_A, \theta_\mu\}, \tag{4.1}$$

where $m_{1/2}$ and m_0 are the GUT-scale universal gaugino and scalar masses, respectively. The magnitude of the μ-parameter and the pseudoscalar mass are determined by the radiative electroweak symmetry breaking conditions. We will present the analysis separately for each of the two physical phases, θ_μ and θ_A, which are present under these assumptions.

Let us recall that RG running from the GUT scale in this scenario introduces considerable mass splittings in the spectrum of superpartners; for example, the gluino becomes much heavier than (roughly triple) the rest of the gauginos, while the squarks also become quite heavy, $m_{\text{sq}}^2(M_Z) \simeq m_0^2 + 6m_{1/2}^2 + O(M_Z^2)$. Of particular impor-

tance here, as emphasized above, is that the physical phases also run, and mix, under the RG. The two-loop RGE for the μ parameter is real, and therefore the phase of μ does not run; its low energy value is equal to its input value at the GUT scale. On the other hand, the phases of all of the A parameters do run and are primarily affected by the 3rd generation Yukawa couplings. As discussed earlier, although we are free to set the phases of the gaugino masses to zero at the GUT scale, the 2-loop RGEs induce phases for $M_{1,2,3}$ when the phases of A are not zero. The mixing of physical phases that this induces will be illustrated below.

In what follows, we present our numerical results for the EDMs in the context of the CMSSM.

1. Phase constraints in benchmark scenarios

Detailed phenomenological studies have found it useful to concentrate on very specific CMSSM parameter choices. To this end, several sets of benchmark points have been established [65–67]. A set of proposed post-LEP benchmark scenarios [65] were chosen to span the CMSSM parameter space in regions where all phenomenological constraints are satisfied. These include obtaining a cosmological relic density with the limits established by Wilkinson Microwave Anisotropy Probe (WMAP) [68]. Several points were chosen to lie in the "bulk" region at small $m_{1/2}$ and m_0, while others are spread along either the $\chi - \tilde{\tau}$ coannihilation "tail" at larger $m_{1/2}$ or in rapid-annihilation "funnels" where the relic density is controlled by s-channel annihilation of the lightest supersymmetric particle (LSP) through the heavy Higgs scalar and pseudoscalar at large $m_{1/2}$ and m_0 at large $\tan\beta$.

We begin our analysis, therefore, with a discussion of EDMs in the context of four selected benchmark scenarios. Point B is a bulk point with $(m_{1/2}, m_0, \tan\beta) = (250, 75, 10)$. The value of m_0 is shifted slightly (+ 15 GeV) from [67] due the larger value of the top quark mass (we adopt $m_t = 178$ GeV as opposed to 175 GeV used previously) and to several improvements in the spectrum code, most notably the inclusion of the full set of 2-loop RGEs. Note that here we have also chosen $A_0 = 300$ GeV as opposed to 0, to allow for effects with nonzero phases. This also adds to the shift in m_0. In Fig. 3(a), we show the magnitude of the EDMs for benchmark point B in a plane defined by the phases of A_0 and μ. Within the blue shaded region the Tl EDM is less than or equal to its current experimental limit. The blue (dashed) contours show the values of phases when the Tl EDM exceeds its experimental bound by a factor of 10 and 50. The black (dashed) curve within the shaded region has $d_{\text{Tl}} = 0$. Similarly, within the red shaded region the neutron EDM is within its experimental bound. The red dotted curve corresponds to a neutron EDM which is 10 times the experimental limit. Finally, the green shaded region displays the Hg EDM bound and the green (solid) curves

---

[2]Note that additional 2-loop threshold corrections, such as Fig. 1(b) [29], can in principle be larger than the Barr-Zee type contributions, and thus a full analysis of 2-loop threshold corrections appears warranted. However, within the CMSSM, we have verified that the complex wave function-induced correction Σ [29] to the chargino mass matrix is, even when non-negligible compared to other conventional sources, still generally subleading relative to complex 2-loop RG corrections to the 1-loop diagrams.
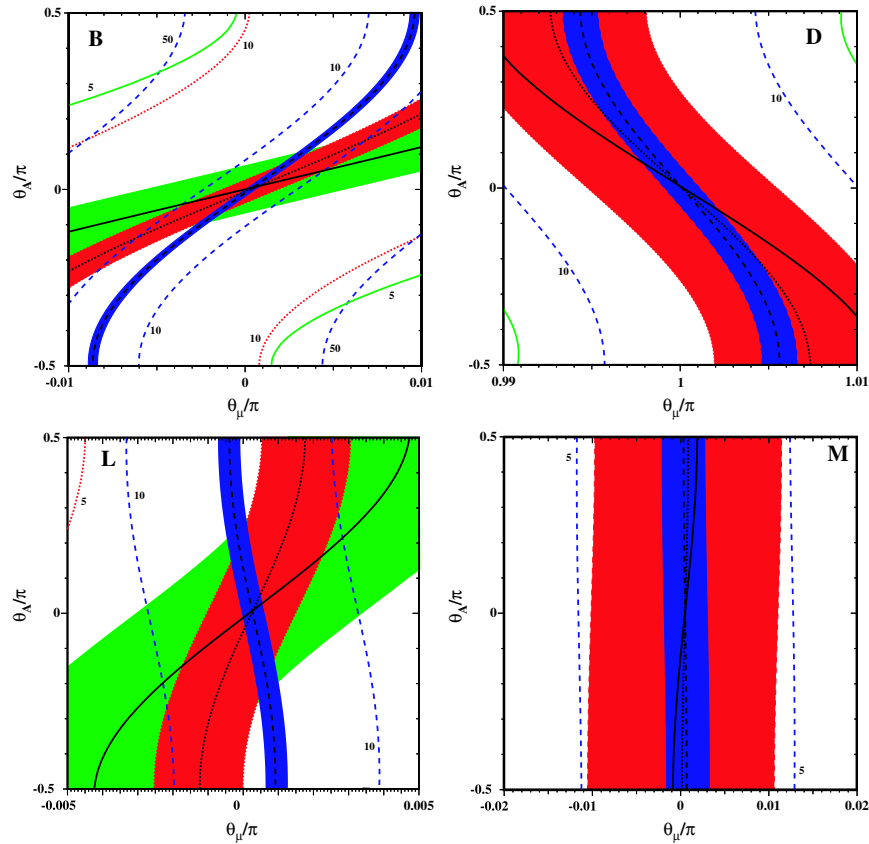
FIG. 3 (color online). The Tl (blue dashed line), neutron (red dotted line), and Hg (green solid line) EDMs relative to their respective experimental limits in the θ_μ, θ_A plane for benchmark points B, D, L, and M. Inside the shaded regions, the EDMs are less than or equal to their experimental bounds. Each of the EDMs vanish along the black contour within the shaded region.

shows where the Hg EDM is 5 times its experimental limit. As expected, the bounds on θ_μ are far stronger than those on θ_A. However, because the EDMs cut the phase planes differently, when limits to all three EDMs are applied, a relatively strong limit ($|\theta_A/\pi| \lesssim 0.08$) can be obtained in this case. The limit on $|\theta_\mu|$ is approximately 0.002π.

In Fig. 3(b), we show the result for benchmark point D, which is a point along the $\chi - \tilde{\tau}$ coannihilation tail and (in the absence of phases) has $\mu < 0$ with $(m_{1/2}, m_0, \tan\beta) = (525, 130, 10)$, applying a 20 GeV shift in m_0. In this case, the sparticle masses are generally larger than found for point B, primarily due to the increase in $m_{1/2}$. Here, we do not show the shaded region obtained from the Hg EDM as it would fill the displayed plane. The Hg contours in the upper right and lower left of the panel show where the EDM is equal to its experimental limit. For point D, we find no limit to θ_A, while $|\theta_\mu - \pi| \lesssim 0.065\pi$.

Point L [shown in Fig. 3(c)] is also a coannihilation point, at large $\tan\beta$. Point L is defined by $(m_{1/2}, m_0, \tan\beta) = (450, 355, 50)$. In this case, because $\tan\beta$ is large, we applied a larger shift (55 GeV) in m_0 to obtain the correct relic density when phases are absent. Once again, we recover a bound on θ_A, albeit a weak one of about 0.2π. In this case, we have a very strong constraint

on θ_μ, $|\theta_\mu| \lesssim 0.0005\pi$. Finally, point M, shown in Fig. 3(d), is also a large $\tan\beta$ point found high in the funnel region with $(m_{1/2}, m_0, \tan\beta) = (1500, 1100, 57)$. Because the funnel region is very sensitive to $\tan\beta$, $m_{1/2}$, and m_t, we increased $\tan\beta$ from 50 to 57, and lowered $m_{1/2}$ from 1840 GeV to 1500 GeV. As for point D, we do not show the shaded region for the Hg EDM (as it would fill the plane as displayed). As one can see, there is no bound on θ_A, and despite the large values of $m_{1/2}$ and m_0, there is still a significant bound on $|\theta_\mu|$ of 0.004π.

The constraints for all four benchmark scenarios are summarized in Table I.

TABLE I. A summary of the constraints on the phases within the four benchmark scenarios shown in Fig. 3. All points use $|A_0| = 300$ GeV, and the quoted bound on the phase of μ for point D is modulo π.

Benchmark point $(m_{1/2}, m_0, \tan\beta)$	$|\theta_A/\pi|$	$|\theta_\mu/\pi|$
B (250,75,10)	$\lesssim 0.08$	$\lesssim 0.002$
D (525 130 10)	$\cdots$	$\lesssim 0.07$
L (450 355 50)	$\lesssim 0.2$	$\lesssim 0.0005$
M (1500 1100,57)	$\cdots$	$\lesssim 0.004$

2. General constraints on the CMSSM parameter space

We now turn to a more general analysis of the CMSSM $(m_{1/2}, m_0)$ plane for fixed values of $\tan\beta$. We will present the results in several different ways. One motivation for restricting our attention to the CMSSM is that we can subject the theory to a full suite of different phenomenological constraints. On the following parameter space plots we will indicate the excluded and preferred regions due to the following:

LSP dark matter: Regions in parameter space where the LSP is charged, generically a stau, are not viable and can be excluded. Moreover, if one demands that the relic density is consistent with the range $\Omega h^2 = 0.0945$–0.1287 determined by WMAP [68], this limits the viable region to thin strips in the $(m_{1/2}, m_0)$ plane. Furthermore, the relic density is generically too large on one side of the WMAP strip. We will calculate this relic density in the absence of phases, but will restrict the magnitude of the phases so that their impact should be negligible [15,16].

Contributions to $b \rightarrow s\gamma$: Within the flavor sector, constraints on the supersymmetric contributions to $b \rightarrow s\gamma$ are often important for low values of $m_{1/2}$, particularly at large $\tan\beta$ [69].

LEP chargino and Higgs searches: The constraints resulting from the null LEP results for Higgs [70] and chargino [71] searches also impinge on the CMSSM parameter space for small $m_{1/2}$.

Our motivation is not to search specifically for regions allowed by all of these constraints, but to emphasize the complementarity of the constraints, and the relative importance of those imposed by EDMs. The resulting conclusions should then be relevant, qualitatively at least, in more general SUSY-breaking scenarios.

In presenting our results, we will consider the contribution of the two phases separately, and we will also use two phase values of $\pi/20$ and $\pi/6$, and show contour plots of $d/d_{\rm exp}$, the EDM relative to its current experimental bound (or future level of sensitivity). These phases are both within the linear regime and thus the contours can easily be converted to bounds on the phases, $\theta \lesssim \theta_0/(d/d_{\rm exp})$, where θ_0 denotes the nonzero phase chosen for the plot. This allows for a simple rescaling of our results given updated future limits.

The smaller phase value $\pi/20$ was chosen to restrict attention the phenomenologically most interesting region, where the spectrum is not highly tuned. Note that the tuning of this phase is comparable to the minimal tuning that must be imposed on the spectrum in the CMSSM, as implied by the LEP bounds and the electroweak precision tests (see e.g. [72] for a recent analysis within the MSSM). We have also included results with a "near maximal" phase $\pi/6$ to illustrate the full reach of the EDM constraints with regard to the parameter space of the CMSSM and the SUSY spectrum. The value $\pi/6$ was adopted as the boundary of the linear regime, to allow for a simple interpretation of the contours, and, if viewed as a "maximal" phase, also takes into account a conservative (factor of 2) uncertainty in some of the hadronic EDMs.

We will now present the results in more detail.

Low $\tan\beta$ and future sensitivity.—In Figs. 4(a) and 4(b), we show the current constraints in the CMSSM plane for $\tan\beta = 10$ due to the Tl, neutron, and Hg EDMs for $\theta_A = 0.05\pi$ (a) and $\theta_\mu = 0.05\pi$ (b). As in Fig. 3, the blue (dashed), red (dotted), and green (solid) curves correspond to the Tl, neutron, and Hg EDMs, respectively. As described above, the contour labels show the magnitude of the EDM relative to the current experimental bound. Throughout the $(m_{1/2}, m_0)$ plane, we have taken $m_t = 178$ GeV, $m_b(m_b) = 4.25$ GeV, and $|A_0| = 300$ GeV, with $\theta_A = 0.05\pi$, $\theta_\mu = 0$ in (a), and $\theta_\mu = 0.05\pi$, $\theta_A = 0$ in (b). In each of the panels, the brown shaded region in the lower right corresponds to that portion of the CMSSM plane where the right-handed stau is the LSP, and is therefore excluded. The green shaded region in the left of each panel is also excluded as there the supersymmetric contribution to $b \rightarrow s\gamma$ is too large. Also shown are the current constraints from LEP based on the masses of the chargino (nearly vertical black dashed line) and Higgs boson (red dot-dashed line). Regions to the left of these curves are excluded. The gray shaded wisplike region, corresponds to that portion of the plane where the cosmological relic density lies in the range $\Omega h^2 = 0.0945$–0.1287 as determined by WMAP. Any area above this shaded region is excluded as the relic density is too large. Note that the very thin area *below* the WMAP strip and above the stau LSP region is allowed so long as there is another source for dark matter.

In Fig. 4(a), we show the contours for which each of the three EDMs considered, saturates its experimental bound (curves labeled 1). Regions to the left of (or below) these curves are excluded. The constraints from d_n and $d_{\rm Hg}$ are relatively uniform. However, we see that for the Tl EDM, there is a line through the plane where a cancellation occurs, and $d_{\rm Tl} = 0$. Interestingly enough, despite the relatively low value for $\tan\beta$, this cancellation line can be understood through the impact of 2-loop RG corrections to $\text{Im}M_i$.

To see this, recall that for low $\tan\beta$ the Tl EDM is dominated by 1-loop threshold corrections to d_e, which to a reasonable approximation take the form shown in Eq. (2.1). Since μ is real, the *negative* RG corrections to $\text{Im}M_2$ can lead to a cancellation between the two leading contributions. From (2.7),

$$d_e \propto [5g_2^2 \tan\beta \mu \text{Im}(M_2) + 2g_1^2 \text{Im}(M_1^* A_e)], \qquad (4.2)$$

using the leading-log estimate for $\text{Im}M_2$ in (2.7), and ignoring the subleading imaginary correction to M_1, we can estimate the condition for dominance of the first term in (4.2) as

$$\tan\beta \frac{\mu \text{Im}(A_0)}{M_1 \text{Im}(A_e)} \gtrsim 17 \longrightarrow \tan\beta \gtrsim 7, \qquad (4.3)$$

where in the second relation we have used $|\mu| \sim (-m_{H_2}^2)^{1/2} \sim 1.6 m_{1/2}$, $M_1 \sim 0.4 m_{1/2}$, and $\text{Im}(A_e) \sim 1.6\text{Im}(A_0)$ to provide an indication of the size of $\tan\beta$ needed to achieve a cancellation in the relevant part of the $(m_{1/2}, m_0)$ plane. We see that moderate values of $\tan\beta$ are already sufficient, and indeed this cancellation is apparent in Fig. 4(a). Its precise shape depends on a number of other contributions that we have neglected, which become more important at large $\tan\beta$ as we will discuss below. For completeness, the plot also indicates contours for the EDMs which are 5 times their experimental bound, and one contour for Tl where the EDM is 10 times it experimental value (the innermost of the blue dashed curves).

In contrast, when $\theta_\mu = 0.05\pi$, as in Fig. 4(b), the constraints become much stronger. All the curves are now labeled by the value of d/d_{exp}, i.e. the ratio by which the predicted EDM exceeds the experimental bound. For this choice of θ_μ, we see that the entire region of the plane shown in the figure is excluded. The Tl EDM, which now exhibits no cancellation line as it is dominated by the first term in (2.1), supplies by far the strongest constraint. Nonetheless, d_n and d_{Hg} also provide strong constraints across the plane. As described above, since the phase is small and the contribution to the EDM is thus linear, we can also use the curves to place a limit on θ_μ. For example, the region to the right of the Tl curve labeled 50 is allowed so long as $\theta_\mu \lesssim 0.05\pi/50 = 0.001\pi$. Similarly for the other curves in this panel.

In the lower half of Fig. 4, we consider how the present situation will be modified with the next generation of EDM experiments, and exhibit the anticipated sensitivities. In Figs. 4(c) and 4(d), we show d_e (blue dashed line), the neutron (red dotted line), and the deuteron (black solid line) relative to the anticipated future level of sensitivity as described in Sec. III D. We emphasize that there are several experiments in this list sensitive to d_e, and we have simply
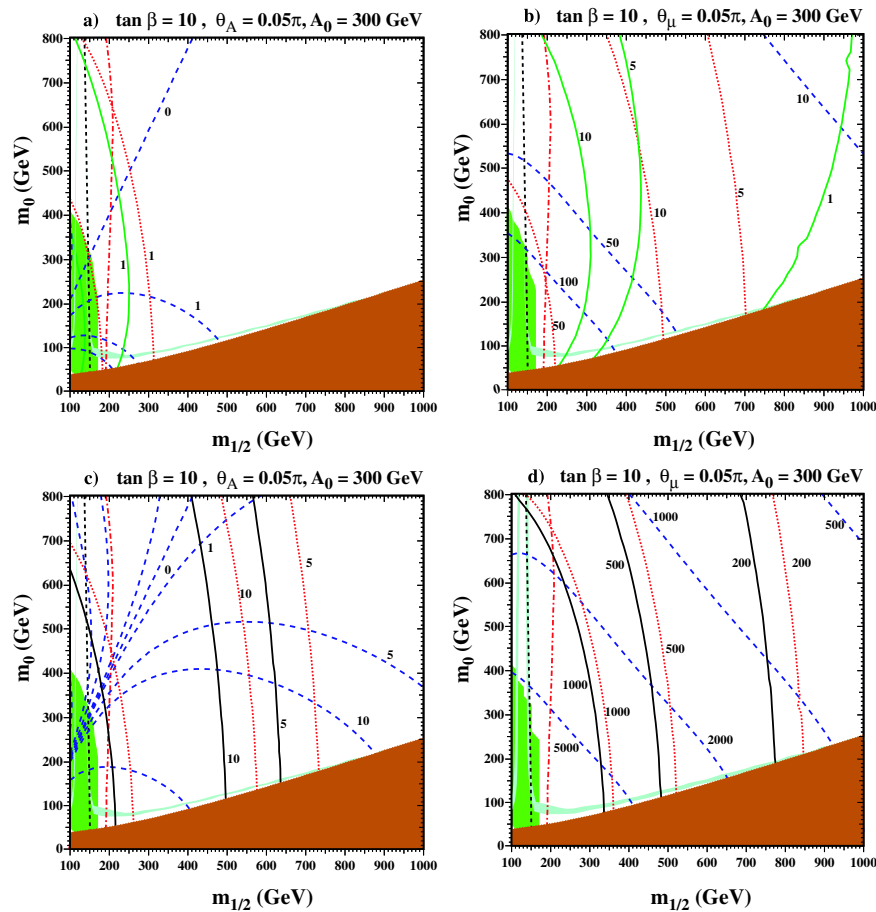

FIG. 4 (color online). The Tl (blue dashed line), neutron (red dotted line), and Hg (green solid line) EDMs relative to their current experimental limits (a,b) and the electron (blue dashed), the neutron (red dotted), and the deuteron (black solid) EDMs relative to possible future experimental limits (c,d) in the $m_{1/2}, m_0$ plane of the CMSSM. In each panel, $|A_0| = 300$ GeV with $\tan\beta = 10$. The shaded regions are described in the text. In (a) and (c), $\theta_A = 0.05\pi$, and in (b) and (d), $\theta_\mu = 0.05\pi$.

deduced the sensitivity to d_e from these, ignoring corrections from electron-nucleon interactions. For small values of $\tan\beta$ as we have here, this should not be a significant problem but one should bear in mind that these conclusions cannot easily be extrapolated to other regimes, e.g. to large $\tan\beta$.

In Fig. 4(c), the contours shown are 5, 10, and 50, where the latter are unlabeled. For d_e, contours of 0 and 1 are also shown. As one can see we expect the deuteron and neutron to give comparable limits which are quite complementary to that obtained from the future bound on the electron EDM from PbO, YbF, etc. As is apparent from the comparison of Figs. 4(a) and 4(c), the limits on the SUSY parameter space are expected to be dramatically improved by future experiments, particularly so for the dependence on θ_A. For $\theta_A = 0.05\pi$, the entire (displayed) plane would be excluded by both the n and D EDMs, provided that future experiments will see zero EDMs, thus forcing a smaller value for the phase of A_0. In Fig. 4(d), we see that the d_e limits become so strong that even at the endpoint of the coannihilation region at $m_{1/2} \simeq 900$ GeV, we are forced to very small phases, $\theta_\mu \lesssim 5 \times 10^{-5}\pi$.

Constraints for large $\tan\beta$.—The large $\tan\beta$ regime exhibits a number of new qualitative features as concerns the dependence on the underlying sources. The 1-loop θ_μ-dependence of the down-type fermions is linearly enhanced, while as we have discussed RG corrections to $\mathrm{Im}M_i$ can similarly provide significant corrections for the dependence on θ_A. A number of 2-loop Barr-Zee type contributions [28,73] to the EDMs and CEDMs are also $\tan\beta$-enhanced and become significant in this regime, while the largest qualitative change arises through the fact that various four-fermion operators provide sizable contributions [26,36,74], and compete with the constituent EDMs. The most prominent example of this is the contribution of C_S to d_{Tl} as described in Sec. III. A comprehensive study of the relative importance of these contributions was carried out in [26], and here we will present combined results for the EDMs within the framework of the CMSSM. It is apparent from the results of [26] that the restrictive ansatz of the CMSSM does not exhibit all the possible regimes that may arise in a more general MSSM scenario, and new qualitative features are restricted primarily to the behavior of d_{Tl}.

Our results are presented in the upper two rows of Fig. 5, for $\tan\beta = 30$ and 57, respectively, and again for cases with either nonzero $\theta_A = 0.05\pi$ or $\theta_\mu = 0.05\pi$. As mentioned, the hadronic EDMs, d_n and d_{Hg}, are still primarily dominated by the one-loop contributions and thus are not altered significantly for nonzero θ_A (cf. Figs. 5(a) and 5(c) with Fig. 4(a)], while they scale up linearly with $\tan\beta$ for nonzero θ_μ (cf. Figs. 5(b) and 5(d) with Fig. 4(b)]. We recall that although the 2-loop RG-induced corrections for nonzero θ_A are present and $\tan\beta$-enhanced, they are not particularly large for the quark EDMs and CEDMs as all

contributions arise predominantly via squark-gluino loops. Indeed, it is apparent from Figs. 5(a) and 5(c) that, for our rather small value of $\theta_A = 0.05\pi$, the EDMs are less constraining than the limits from $b \to s\gamma$. On the plots for $\tan\beta = 57$, one may note the appearance of the funnel-like region where dark matter annihilations are mediated by s-channel heavy Higgs exchange.

Let us now focus our attention on the contours for d_{Tl}. At first sight, the results for $\tan\beta = 30$ may not look dramatically different from those for $\tan\beta = 10$. We see once again a cancellation line extending out now to somewhat larger values of $m_{1/2}$. However, its precise form is now determined by a more complex interplay between many different effects. Indeed, from (4.3) we might expect that the $\mathrm{Im}M_2$-induced corrections would now dominate the 1-loop contribution to d_e. This is indeed the case, but for $\tan\beta = 30$ the 2-loop corrections and the contributions from C_S are also competitive, and the observed cancellation line results from the interplay of all of these sources. It is only for sufficiently large $\tan\beta$, as observed for $\tan\beta = 57$ in Fig. 5(c), that the cancellation line disappears, as the various contributions fall out of balance, although there are still some partial intermediate cancellations [26].

We have not included plots outlining the future sensitivity in this case, due to the lack of atomic calculations detailing the contributions from four-fermion operators for the relevant paramagnetic sources. Nonetheless, by comparison with Fig. 4(c) it should be clear that much of the displayed plane will again be covered by the EDM reach, even for $\theta_A = 0.05\pi$, providing a significant improvement over the current results in Figs. 5(a) and 5(c).

Impact of two-loop RG-evolution of the phases.—To gauge the effect of the inclusion of the 2-loop RGEs, we have also shown in Figs. 5(e) and 5(f) the constraints on the CMSSM plane when only the 1-loop RGEs are run for nonzero θ_A. For clarity, we have only displayed contours with $d = d_{\mathrm{exp}}$. As anticipated in our discussion in Sec. II, the Tl EDM is most affected by the inclusion of the 2-loop RGEs and as one sees, the cancellation line at $\tan\beta = 30$, which using the 1-loop RGEs barely appears on the top left corner of the plot, is rotated clockwise and shifted to close to the middle of the plane. Similarly, for $\tan\beta = 57$, the cancellation that is apparent when using the 1-loop RGEs is shifted into the stau LSP region in Fig. 5(c).

One should bear in mind in viewing these plots that the spectrum is also slightly perturbed in shifting from 1-loop to 2-loop RGEs, but this is a minor effect and the dominant change in the EDMs is due to the induced corrections to $\mathrm{Im}M_i$. The significant shift in the WMAP band is due to the fact that the funnel region is highly sensitive to the pseudoscalar Higgs mass.

Full EDM reach in the CMSSM parameter space.—In the analysis above, we have chosen rather small phases, consistent with the level of implied tuning in the CMSSM,
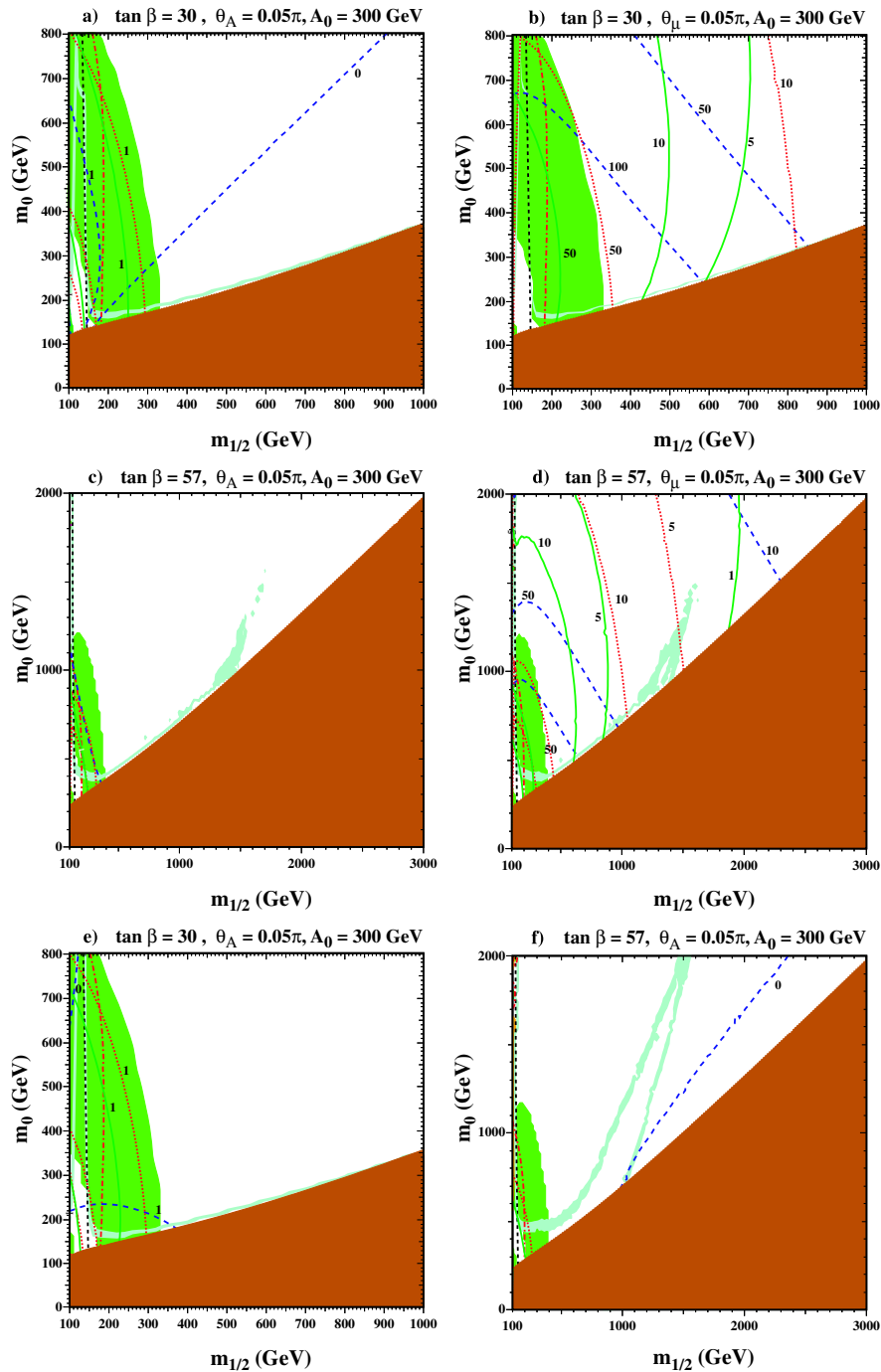
FIG. 5 (color online).   As in Fig. 4, the Tl (blue dashed line), neutron (red dotted line), and Hg (green solid line) EDMs relative to their current respective experimental limits in the $m_{1/2}$, m_0 plane of the CMSSM for $\tan\beta = 30$ (a), (b), and (e), and $\tan\beta = 57$ (c), (d), and (f). In each panel, $|A_0| = 300$ GeV. In (a), (c), (e), and (f), $\theta_A = 0.05\pi$, and in (b) and (d), $\theta_\mu = 0.05\pi$. In panels (e) and (f) only 1-loop RGEs were used to compute the supersymmetric particle spectrum.

to focus in on the phenomenologically most interesting region. However, it is also clearly of interest to determine precisely how far the EDMs can reach in terms of the parameter space of the CMSSM, and more generally in terms of the sparticle spectra. Thus, we will now boost the phases to $\pi/6 \sim 0.17\pi$, which we will take as the bound-

ary of the linear domain, so that we can still use the figures to approximate the limit on the given phase at any specific point in the CMSSM plane. As discussed earlier, if $\pi/6$ is taken as a maximal phase value, it also provides a conservative treatment of some of the calculational uncertainties.

Our results are shown in Fig. 6, where the current (Figs. 6(a) and 6(b)) and future (Figs. 6(c) and 6(d)) contours are shown for both θ_A (a and c) and θ_μ (Figs. 6(b) and 6(d)). Here we show only the value of the EDM relative to its experimental limit and suppress the other cosmological and phenomenological constraints. Where possible, contours of 0, 1, 5, 10, 50, and 100 are shown. Note that the shaded region in the upper left corner of each panel above the solid black curve is not viable in the CMSSM as there are no solutions which allow for radiative electroweak symmetry breaking. (The boundary zone near this line is often called the focus point region, or the hyperbolic branch.) When $\theta_A = 0.17\pi$ and $\theta_\mu = 0$, we see from Fig. 6(a) that the reach is not terribly strong. For comparison, we show the expected reach of the LHC based on its ability to detect colored sparticles with masses up to 2 TeV [75,76]. However, we observe that the future sensitivity of the neutron and deuteron EDM experiments will extend beyond the reach of the LHC for $m_0 \lesssim 4.5$ TeV. While it is

interesting that the cancellation line apparently weakens the constraints from paramagnetic sources, we emphasize that corrections from four-fermion sources may change this significantly in the case of PbO and YbF, and that this cancellation may not survive in more general variants of the MSSM.

In contrast, when $\theta_\mu = 0.17\pi$, the current reach of all three EDM experiments already exceeds the projected reach of the LHC as seen in Fig. 6(b). For completeness, we show in Fig. 6(d) the expected reach from future EDM experiments. This figure shows that for large θ_μ the EDMs can be sensitive to superpartner mass scales as high as a few tens of TeV. While such scenarios are apparently highly tuned, one may try to rescue naturalness via SUSY-breaking mechanisms, outside the CMSSM framework, where only the first two generation scalars are pushed above 10 TeV in order to cure the SUSY flavor problem by "brute force," while keeping the 3rd generation scalars light in order not to exacerbate the fine-tuning
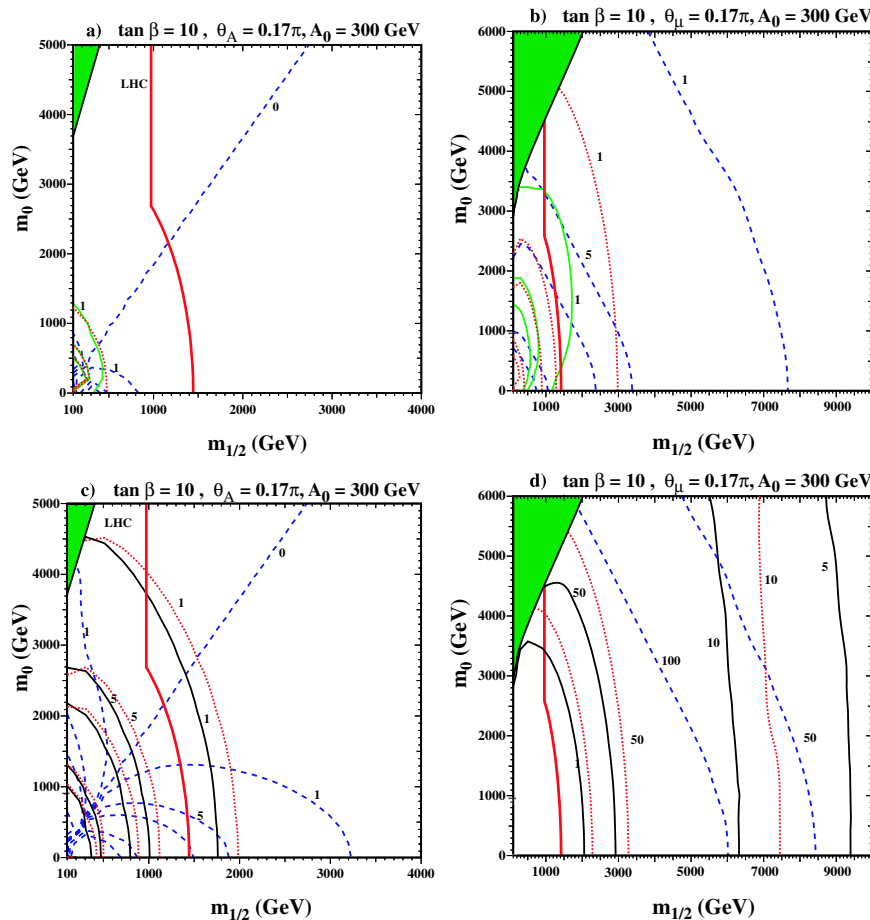

FIG. 6 (color online). As in Fig. 4, the Tl (blue dashed line), neutron (red dotted line), and Hg (green solid line) EDMs relative to their current experimental limits (a,b) and the electron (blue dashed line), the neutron (red dotted line), and the deuteron (black solid line) EDMs relative to possible future experimental limits (c,d) in the $m_{1/2}, m_0$ plane of the CMSSM for $\tan\beta = 10$. In each panel, $|A_0| = 300$ GeV. In (a) and (c), $\theta_A = 0.17\pi$, and in (b) and (d), $\theta_\mu = 0.17\pi$.

problem in the Higgs sector [22]. It is clear that the next-generation EDM searches will directly probe such scenarios.

The shape of these contours is easily understood given the large RG-induced admixture of $m_{1/2}$ to the squark masses. We see that the contours for the hadronic EDMs are squashed towards the m_0 axis as a consequence of the rapid suppression of the EDMs as $m_{1/2}$ becomes large. This effect is absent for the paramagnetic EDM bounds, and we observe a more uniform shape for these contours.

V. CONCLUDING REMARKS

We have performed a general analysis of the EDM constraints on the CMSSM parameter space, combining a number of weak-scale threshold contributions to the fermion EDMs and CEDMs, and also four-fermion operators. The latter contributions are generally subleading, but become important at large $\tan\beta$ and must be taken into account for a complete analysis of this regime. We have emphasized two main points as part of this analysis. First, as the experimental situation is rapidly evolving, we have presented estimates for the sensitivity of the next generation of EDM experiments in each of the three sectors which currently provide the strongest constraints, namely, paramagnetic sources sensitive to the electron EDM, and the neutron and deuteron which are sensitive to (different) combinations of quark/gluon operators. The most striking impact of the expected levels of improvement in sensitivity is that the reach of EDMs induced by θ_A increases significantly, to the extent that it exceeds that of the LHC for large phases. The reach in terms of θ_μ already probes superpartner mass scales that cannot be directly accessed at the LHC.

The second point, of technical importance, that we have emphasized is that 2-loop RG-induced corrections to ImM_i can significantly enhance the dependence of the electron EDM to θ_A, particularly so at large $\tan\beta$. While on first inspection it would appear that these RG-induced contributions generically dominate the Tl EDM by a factor of a few, it turns out that the relative signs are such that significant cancellations occur, and the bounds are often weakened, at least for moderate $\tan\beta$. For large $\tan\beta$, a number of different contributions become competitive, but on closer inspection one may observe by comparing Figs. 5(c) and 5(f) that the constraints from Tl do in fact become stronger with the inclusion of the RG-induced corrections, although overall they remain relatively weak in this regime. A summary of some of the constraints on the phases in specific benchmark scenarios is shown in Table I.

A natural question is whether these conclusions will hold in more general examples of the MSSM, where a number of the universality assumptions are lifted, and the number of independent phases is correspondingly increased. While the most recent explorations of this kind [20,21,26] suggest that the picture is not dramatically modified, this is clearly a question worthy of further study.

ACKNOWLEDGMENTS

[1] P. G. Harris *et al.*, Phys. Rev. Lett. **82**, 904 (1999).

[2] B. C. Regan, E. D. Commins, C. J. Schmidt, and D. DeMille, Phys. Rev. Lett. **88**, 071805 (2002).

[3] M. V. Romalis, W. C. Griffith, and E. N. Fortson, Phys. Rev. Lett. **86**, 2505 (2001).

[4] D. Cho, K. Sangster, and E. A. Hinds, Phys. Rev. Lett. **63**, 2559 (1989).

[5] M. A. Rosenberry and T. E. Chupp, Phys. Rev. Lett. **86**, 22 (2001).

[6] S. A. Murthy, D. Krause, Jr., Z. L. Li, and L. R. Hunter, Phys. Rev. Lett. **63**, 965 (1989).

[7] J. J. Hudson, B. E. Sauer, M. R. Tarbutt, and E. A. Hinds, Phys. Rev. Lett. **89**, 023003 (2002).

[8] D. DeMille *et al.*, Phys. Rev. A **61**, 052507 (2000).

[9] I. B. Khriplovich and S. K. Lamoreaux, *CP Violation Without Strangeness* (Springer, Berlin 1997).

[10] J. R. Ellis, S. Ferrara, and D. V. Nanopoulos, Phys. Lett. **114B**, 231 (1982); W. Buchmuller and D. Wyler, Phys. Lett. **121B**, 321 (1983); J. Polchinski and M. B. Wise, Phys. Lett. **125B**, 393 (1983); M. Dugan, B. Grinstein, and L. J. Hall, Nucl. Phys. **B255**, 413 (1985).

[11] R. N. Mohapatra and G. Senjanovic, Phys. Lett. **79B**, 283 (1978); S. M. Barr, Phys. Rev. Lett. **53**, 329 (1984); A. E. Nelson, Phys. Lett. **136B**, 387 (1984).

[12] S. Dimopoulos and S. Thomas, Nucl. Phys. **465B**, 23 (1996); R. Kuchimanchi, Phys. Rev. Lett. **76**, 3486 (1996); R. N. Mohapatra and A. Rasin, Phys. Rev. Lett. **76**, 3490 (1996); M. E. Pospelov, Phys. Lett. B **391**, 324 (1997); G. Hiller and M. Schmaltz, Phys. Lett. B **514**, 263 (2001).

[13] S. Abel, S. Khalil, and O. Lebedev, Phys. Rev. Lett. **89**, 121601 (2002).

[14] R. Barbieri, L. J. Hall, and A. Strumia, Nucl. Phys. **B445**, 219 (1995); I. B. Khriplovich and K. N. Zyablyuk, Phys. Lett. B **383**, 429 (1996); J. Hisano and Y. Shimizu, Phys. Lett. B **581**, 224 (2004); S. Abel and S. Khalil, Phys. Lett.

B **618**, 201 (2005).

[15] T. Falk and K. A. Olive, Phys. Lett. B **375**, 196 (1996).

[16] T. Falk and K. A. Olive, Phys. Lett. B **439**, 71 (1998).

[17] T. Ibrahim and P. Nath, Phys. Lett. B **418**, 98 (1998); Phys. Rev. D **57**, 478 (1998); **58**, 019901(E)(1998); **60**, 079903(E) (1999); **60**, 119901(E) (1999); **58**, 111301 (1998); **60**, 099902(E) (1999).

[18] M. Brhlik, G. J. Good, and G. L. Kane, Phys. Rev. D **59**, 115004 (1999); M. Brhlik, L. L. Everett, G. L. Kane, and J. Lykken, Phys. Rev. Lett. **83**, 2124 (1999); A. Bartl, T. Gajdosik, W. Porod, P. Stockinger, and H. Stremnitzer, Phys. Rev. D **60**, 073003 (1999); S. Pokorski, J. Rosiek, and C. A. Savoy, Nucl. Phys. **B570**, 81 (2000); R. Arnowitt, B. Dutta, and Y. Santoso, Phys. Rev. D **64**, 113010 (2001).

[19] T. Falk, K. A. Olive, M. Pospelov, and R. Roiban, Nucl. Phys. **B560**, 3 (1999).

[20] V. D. Barger, T. Falk, T. Han, J. Jiang, T. Li, and T. Plehn, Phys. Rev. D **64**, 056007 (2001).

[21] S. Abel, S. Khalil, and O. Lebedev, Nucl. Phys. **B606**, 151 (2001).

[22] P. Nath, Phys. Rev. Lett. **66**, 2565 (1991); Y. Kizukuri and N. Oshimo, Phys. Rev. D **45**, 1806 (1992); **46**, 3025 (1992); A. G. Cohen, D. B. Kaplan, and A. E. Nelson, Phys. Lett. B **388**, 588 (1996).

[23] T. Falk, K. A. Olive, and M. Srednicki, Phys. Lett. B **354**, 99 (1995).

[24] J. R. Ellis, K. A. Olive, Y. Santoso, and V. C. Spanos, Phys. Lett. B **565**, 176 (2003); Phys. Rev. D **69**, 095004 (2004).

[25] V. D. Barger and C. Kao, Phys. Lett. B **518**, 117 (2001); L. Roszkowski, R. Ruiz de Austri, and T. Nihei, J. High Energy Phys. 08 (2001) 024; A. B. Lahanas and V. C. Spanos, Eur. Phys. J. C **23**, 185 (2002); A. Djouadi, M. Drees, and J. L. Kneur, J. High Energy Phys. 08 (2001) 055; U. Chattopadhyay, A. Corsetti, and P. Nath, Phys. Rev. D **66**, 035003 (2002); H. Baer, C. Balazs, A. Belyaev, J. K. Mizukoshi, X. Tata, and Y. Wang, J. High Energy Phys. 07 (2002) 050; R. Arnowitt and B. Dutta, hep-ph/0211417; H. Baer and C. Balazs, J. Cosmol. Astropart. Phys. 05 (2003) 006; A. B. Lahanas and D. V. Nanopoulos, Phys. Lett. B **568**, 55 (2003); U. Chattopadhyay, A. Corsetti, and P. Nath, Phys. Rev. D **68**, 035005 (2003); C. Munoz, Int. J. Mod. Phys. A **19**, 3093 (2004); R. Arnowitt, B. Dutta, and B. Hu, hep-ph/0310103.

[26] D. A. Demir, O. Lebedev, K. A. Olive, M. Pospelov, and A. Ritz, Nucl. Phys. **B680**, 339 (2004).

[27] R. Garisto and J. D. Wells, Phys. Rev. D **55**, 1611 (1997).

[28] D. Chang, W. Y. Keung, and A. Pilaftsis, Phys. Rev. Lett. **82**, 900 (1999); **83**, 3972(E) (1999); A. Pilaftsis, Phys. Lett. B **471**, 174 (1999).

[29] A. Pilaftsis, Phys. Rev. D **62**, 016007 (2000).

[30] Y. Yamada, Phys. Lett. B **316**, 109 (1993); S. P. Martin and M. T. Vaughn, Phys. Lett. B **318**, 331 (1993); Phys. Rev. D **50**, 2282 (1994).

[31] M. Pospelov and A. Ritz, Ann. Phys. (N.Y.) **318**, 119 (2005).

[32] V. M. Khatsimovsky, I. B. Khriplovich, and A. S. Yelkhovsky, Ann. Phys. (N.Y.) **186**, 1 (1988).

[33] V. M. Khatsymovsky and I. B. Khriplovich, Phys. Lett. B **296**, 219 (1992).

[34] X. G. He and B. McKellar, Phys. Lett. B **390**, 318 (1997).

[35] C. Hamzaoui and M. Pospelov, Phys. Rev. D **65**, 056002 (2002).

[36] O. Lebedev and M. Pospelov, Phys. Rev. Lett. **89**, 101801 (2002).

[37] R. D. Peccei and H. R. Quinn, Phys. Rev. Lett. **38**, 1440 (1977).

[38] Z. W. Liu and H. P. Kelly, Phys. Rev. A **45**, R4210 (1992).

[39] A.-M. Martensson-Pendrill, in *Methods in Computational Chemistry, Vol. 5: Atomic, Molecular Properties*, edited by S. Wilson (Plenum Press, New York 1992).

[40] E. Lindroth and A.-M. Martensson-Pendrill, Europhys. Lett. **15**, 155 (1991).

[41] J. S. M. Ginges and V. V. Flambaum, Phys. Rep. **397**, 63 (2004).

[42] H. Y. Cheng, Phys. Lett. B **219**, 347 (1989); J. Gasser, H. Leutwyler, and M. E. Sainio, Phys. Lett. B **253**, 252 (1991); H. Leutwyler, hep-ph/9609465; B. Borasoy and U. G. Meissner, Ann. Phys. (N.Y.) **254**, 192 (1997); M. Knecht, *Publications of the 8th International Symposium on Meson-Nucleon Physics and the Structure of the Nucleon, 1999* [PiN Newsletter 15, 108 (1999); M. Frink, U. G. Meissner, and I. Scheller, Eur. Phys. J. A **24**, 395 (2005).

[43] P. Schweitzer, Eur. Phys. J. A **22**, 89 (2004).

[44] M. Pospelov and A. Ritz, Phys. Rev. Lett. **83**, 2526 (1999); Nucl. Phys. **B573**, 177 (2000); Phys. Rev. D **63**, 073015 (2001).

[45] D. A. Demir, M. Pospelov, and A. Ritz, Phys. Rev. D **67**, 015007 (2003).

[46] R. J. Crewther, P. Di Vecchia, G. Veneziano, and E. Witten, Phys. Lett. **88B**, 123 (1979); **91B**, 487(E) (1980).

[47] A. Pich and E. de Rafael, Nucl. Phys. **B367**, 313 (1991).

[48] J. Hisano and Y. Shimizu, Phys. Rev. D **70**, 093001 (2004).

[49] D. Chang, T. W. Kephart, W. Y. Keung, and T. C. Yuan, Phys. Rev. Lett. **68**, 439 (1992).

[50] R. Arnowitt, J. L. Lopez, and D. V. Nanopoulos, Phys. Rev. D **42**, 2423 (1990).

[51] L. I. Schiff, Phys. Rev. **132**, 2194 (1963).

[52] V. A. Dzuba, V. V. Flambaum, J. S. M. Ginges, and M. G. Kozlov, Phys. Rev. A **66**, 012111 (2002).

[53] V. F. Dmitriev and R. A. Sen'kov, Yad. Fiz. **66**, 1988 (2003) [Phys. At. Nucl. **66**, 1940 (2003)].

[54] M. Pospelov, Phys. Lett. B **530**, 123 (2002).

[55] S. K. Lamoreaux, nucl-ex/0109014; C. Y. Liu, and S. K. Lamoreaux, Mod. Phys. Lett. A **19**, 1235 (2004).

[56] M. G. Kozlov, J. Phys. B **30**, L607 (1997); M. G. Kozlov and D. DeMille, Phys. Rev. Lett. **89**, 133001 (2002).

[57] Y. K. Semertzidis *et al.* (EDM Collaboration), in *Intersection of Particle and Nuclear Physics*, AIP Conf. Proc. No. 698, (AIP, New York, 2004) p. 200.

[58] I. B. Khriplovich and R. A. Korkin, Nucl. Phys. **A665**, 365 (2000).

[59] O. Lebedev, K. A. Olive, M. Pospelov, and A. Ritz, Phys. Rev. D **70**, 016003 (2004).

[60] C. P. Liu and R. G. E. Timmermans, Phys. Rev. C **70**, 055501 (2004); R. V. Korkin, nucl-th/0504078.

[61] R. Golub and K. Lamoreaux, Phys. Rep. **237**, 1 (1994); S. Lamoreaux *et al.*, in 6th Conference on the Intersections of Particle and Nuclear Physics (CIPANP 97), Big Sky, MT, 1997 (unpublished); See e.g. http://p25ext.lanl.gov/

edm/edm.html.

[62] See e.g. http://minoserv.maps.susx.ac.uk/~nedm/index. htm.

[63] See e.g. http://ucn.web.psi.ch/.

[64] S. Weinberg, Phys. Rev. Lett. **63**, 2333 (1989).

[65] M. Battaglia *et al.*, Eur. Phys. J. C **22**, 535 (2001).

[66] B. C. Allanach *et al.*, in *Proc. of the APS/DPF/DPB Summer Study on the Future of Particle Physics, Snowmass, 2001*, edited by N. Graf [Eur. Phys. J. C **25**, 113 (2002)].

[67] M. Battaglia, A. De Roeck, J. R. Ellis, F. Gianotti, K. A. Olive, and L. Pape, Eur. Phys. J. C **33**, 273 (2004).

[68] C. L. Bennett *et al.*, Astrophys. J. Suppl. Ser. **148**, 1 (2003); D. N. Spergel *et al.*, Astrophys. J. Suppl. Ser. **148**, 175 (2003).

[69] M. S. Alam *et al.*, (CLEO Collaboration), Phys. Rev. Lett. **74**, 2885 (1995); K. Abe *et al.* (BELLE Collaboration), contribution to the 30th International Conference on High-Energy Physics, Osaka, 2000 (unpublished); See also K. Abe *et al.* (Belle Collaboration), hep-ex/0107065;L. Lista (*BABAR* Collaboration), hep-ex/0110010; G. Degrassi, P. Gambino, and G. F. Giudice, J. High Energy Phys. 12 (2000) 009; M. Carena, D. Garcia, U. Nierste, and C. E. M. Wagner, Phys. Lett. B **499**, 141 (2001); D. A. Demir and K. A. Olive, Phys. Rev. D **65**, 034007 (2002); T. Hurth, hep-ph/0106050; F. Borzumati, C. Greub, and Y.

Yamada, Phys. Rev. D **69**, 055005 (2004).

[70] R. Barate *et al.* (LEP Higgs Working Group for Higgs boson searches) (OPAL Collaboration) (ALEPH Collaboration) (DELPHI Collaboration) (L3 Collaboration), Phys. Lett. B **565**, 61 (2003); Report No. LHWG Note/2001-04, ALEPH-2001-057, DELPHI-2001-114, L3-NOTE-2700, OPAL-TN-699, 2001;hep-ex/0107030; Report No. LHWG Note/2002-01 (unpublished); http://lephiggs.web.cern.ch/LEPHIGGS/papers/July2002_SM/index.html;see e.g. J. R. Ellis, G. Ganis, D. V. Nanopoulos, and K. A. Olive, Phys. Lett. B **502**, 171 (2001).

[71] (Joint LEP 2 Supersymmetry Working Group), Combined LEP Chargino Results, up to 208 GeV, http://lepsusy.web.cern.ch/lepsusy/www/inos_moriond01/charginos_pub.html.

[72] S. Heinemeyer, W. Hollik, and G. Weiglein, hep-ph/0412214.

[73] A. Pilaftsis, Nucl. Phys. **B644**, 263 (2002).

[74] S. M. Barr, Phys. Rev. Lett. **68**, 1822 (1992); Phys. Rev. D **47**, 2025 (1993).

[75] H. Baer, C. Balazs, A. Belyaev, T. Krupovnickas, and X. Tata, J. High Energy Phys. 06 (2003) 054.

[76] J. R. Ellis, K. A. Olive, Y. Santoso, and V. C. Spanos, Phys. Lett. B **603**, 51 (2004).